# Pyrogenic carbon content of *Sphagnum* peat soils estimated using diffuse reflectance FTIR spectrometry

Dominic M. Uhelski[1], Evan S. Kane[1,2], Rodney A. Chimner[1],
Katherine A. Heckman[2], Jessica Miesel[3], Li Xie[4]

[1] College of Forest Resources and Environmental Science, Michigan Technological University, Houghton MI, USA
[2] Northern Research Station, United States Department of Agriculture (USDA), Houghton MI, USA
[3] Department of Plant, Soil and Microbial Sciences, Michigan State University, East Lansing MI, USA
[4] Department of Chemistry, Michigan State University, East Lansing MI, USA

_____

## SUMMARY

Quantifying historical patterns of fire regimes in peatlands can help contextualise current fire behaviour and aid in planning on ecosystem and landscape scales. However, current methods for detecting the evidence of past fires in peat soils are laborious or expensive. Our goal was to develop an effective and inexpensive method for detecting pyrogenic carbon (PyC) concentration in peat which could be used to estimate the occurrence of fires by analysis of discrete soil samples. We correlated diffuse reflectance Fourier-transform infrared spectrometry (FTIR) measurements of peat, and admixtures of peat and PyC, with nuclear magnetic resonance spectrometry (NMR) estimates of PyC concentrations. We compared two methods for modelling PyC concentration based on FTIR data, namely peak fitting and partial least squares regression. Peak fitting analyses of FTIR spectra isolated 15 unique spectral features within the peat matrices, of which five were statistically relevant to PyC detection. Peak-fitting and partial least squares regression modelling both reliably predicted peat sample PyC concentrations, though partial least squares regression needs additional work before a general model can be developed. Therefore, FTIR spectrometry could be used to detect the presence of past fire events within peat soil profiles with relatively low cost and time investment.

**KEY WORDS:** black carbon, Histosol, wildfire

_____

## ABBREVIATIONS

| | |
|---|---|
| FTIR | **F**ourier-**T**ransform **I**nfra-**R**ed, a type of spectrometry |
| DRIFT | **D**iffuse **R**eflectance **FTIR** spectrometry |
| NMR | **N**uclear **M**agnetic **R**esonance spectrometry |
| DP | **D**irect **P**olarisation, a method of NMR spectra acquisition |
| CPTOSS or CP | **C**ross **P**olarisation (with **To**tal **S**pinning **S**ideband suppression), another method of NMR spectra acquisition |
| PyC | **P**yrogenic **C**arbon |
| PLSR | **P**artial **L**east **S**quares **R**egression |
| RMSE | **R**oot **M**ean **S**quare **E**rror, a measure of model accuracy |
| PRESS | **P**redicted **Re**sidual **S**um of **S**quared Error, a measure of model predictive accuracy |

# INTRODUCTION

Peatlands represent a globally significant carbon (C) stock containing 545–1055 Pg C (Nichols & Peteet 2019). While these stocks generally accumulate over long periods of time, changes in climate and disturbance regimes, including increases in the extent and severity of wildfires, threaten the stability of peatland C stocks (Turetsky *et al.* 2015, Goldstein *et al.* 2020). Wildfires are also important in structuring plant communities in peatlands (Benscoter *et al.* 2015) and fire has been used as a management tool in these ecosystems (Farage *et al.* 2009), though not without controversies (Harper *et al.* 2018, Ashby & Heinemeyer 2021). Despite the importance of fire in peatlands there is little information available regarding natural peatland fire regimes due to the difficulties of discerning fire frequencies in peatlands (cf., Kasin *et al.* 2013). Therefore, a quick and affordable method of quantifying historical fire patterns in peatlands would be beneficial to expand the depth and scope of fire research in these ecosystems.

The basic method for discerning fire frequencies in peatlands is to identify the occurrence of pyrogenic carbon (PyC), also called char or black carbon (BC), in accumulated strata within a peat soil profile or nearby sediments (cf., Clark & Hussey 1996). Pyrogenic C encompasses a range of organic compounds which range from barely altered organic matter to completely condensed graphitic carbon (Goldberg 1985, Masiello 2004). There are many techniques that have been used for identifying PyC, with varying degrees of specificity and resource requirements (Schmidt *et al.* 2001, Hammes *et al.* 2007). Organic soils offer a particular challenge in PyC detection because of chemical similarities between peat and the products of burning (Hedges *et al.* 2000), though some chemo-oxidative methods such as the modified weak nitric acid digestion (a.k.a. KMD) method and the dichromate oxidation + Soxhlet extraction methods have had success in isolating PyC in organic horizons (Kaal *et al.* 2007, Knicker *et al.* 2007, Hatten & Zabowski 2009, Maestrini & Miesel 2017). However, it is difficult to quantify artefacts from chemically and/or thermally oxidising methods for PyC detection in organic matrixes (Hammes *et al.* 2007), and time-consuming laboratory procedures with toxic or otherwise dangerous reagents are still required. Microscopy is often used in palaeoecology to identify pollen and PyC particles in organic soils, but such studies are typically limited to only a few cores due to the time it takes to use this technique (Markgraf & Huber 2010, Gałka *et al.* 2015, Crausbay *et al.* 2017).

Microscopic methods have limited potential for analysis beyond evaluating particle morphology and colour, neither of which is exclusive to or necessarily consistent in PyC, though methods exist which attempt to ease the process via chemical treatments to deflocculate, bleach or digest sample matter to aid particle discrimination. Nuclear magnetic resonance (NMR) spectrometry is a useful method for identifying and quantifying PyC in organic matrixes such as peat (Baldock *et al.* 2004, Kaal *et al.* 2007, Ding & Rice 2012, Leifeld *et al.* 2018). However, NMR is expensive and time-consuming, which greatly limits the number of samples that can be processed. Benzene polycarboxylic acid (BPCA) and hydrogen pyrolysis (hypy) both have potential to work in peat soils but, like NMR and microscopy, have limited application due to long processing times (Cotrufo *et al.* 2016 and references within).

In contrast to these methods, Fourier-transform infra-red (FTIR) spectrometry is relatively inexpensive to run, does not involve caustic reagents or complex laboratory procedures, and can have higher sample throughput. FTIR has been used to study a variety of organic materials and processes including wood decay (Pandey & Pitman 2003), soil organic matter (Chen *et al.* 2002, Demyan *et al.* 2012, Margenot *et al.* 2017, Matamala *et al.* 2017), peat decomposition, humification, and recalcitrance (Prasad *et al.* 2000, Artz *et al.* 2006, Artz *et al.* 2008, Hodgkins *et al.* 2018), pyrolysis (Guo & Bustin 1998, Merino *et al.* 2015), and PyC in upland soils (Nocentini *et al.* 2010, Cotrufo *et al.* 2016, Hardy *et al.* 2017). FTIR was recently used to detect PyC in wetland lagoon sediments (Cadd *et al.* 2020). Despite these advancements, to our knowledge FTIR has not yet been applied to identifying PyC in peat. In this study we evaluated the efficacy of FTIR spectrometry to quantify admixtures of PyC generated in peatland wildfires and hemic and sapric peat, as validated with NMR spectrometry.

# METHODS

## Admixture preparation

We produced six sets of admixtures using three different sources of naturally produced PyC (to capture real-world PyC variability) and two peat sources representing shallow (recently living and senescent moss, 0–40 cm) and deep (humified peat, > 40 cm) depth classes taken from *Sphagnum* peatlands. Both types of peat were composites made from *Sphagnum* peat of the appropriate depth. Composites were used to incorporate characteristics of multiple peatlands and microforms and thereby

maximise the generalisability of the models. The surface peat was a composite of surficial *Sphagnum* that was harvested from peatlands in central Alberta (Bourgeau-Chavez *et al.* 2020). The deep peat was a composite of hemic to sapric *Sphagnum* peat that was harvested from peatlands in the Upper Peninsula of Michigan (Chimner *et al.* 2014). We dried the peat samples at 60 °C until they reached constant mass before grinding them in a Wiley mill. We then ground subsamples of the peat in a ball mill until the peat was pulverised. We acquired the three samples of naturally produced PyC from peat using forceps and a dissecting microscope to obtain material visually apparent as PyC from recent fire events. We did not further isolate or concentrate the PyC. The three PyC samples come from evident char layers found in northwestern Canadian peatlands (Bourgeau-Chavez *et al.* 2020), Minnesota (Potvin *et al.* 2015) and Michigan (Bess *et al.* 2014) peatland sites. We ground the PyC using a mortar and pestle and mixed it with the previously ball-milled peat to make admixture series with every combination of PyC and peat matrix. The admixture intervals were 0, 5, 15, 30, 50, 75 and 100 % (visually) apparent PyC by mass fraction. We did not produce admixtures containing 75 % PyC for the Canadian char due to lack of material. We did not duplicate endmembers of 0 % PyC to avoid skewing the regression. We did not include the three PyC endmembers in modelling as, while they do represent natural chars, they had been separated from peat and their spectra would therefore not be representative of a natural char layer in a peat core. Furthermore, we used eight naturally occurring char layers from three different field sites in the Upper Peninsula of Michigan. The maximum total number of samples we used to fit models was (2 peats (shallow, deep)) × (3 PyC sources) × (5 rates (5, 15, 30, 50, 75)) + (2 for shallow and deep peat endmembers) - (2 analyses for the two peat depths with no 75 % PyC Canadian char) = 30 admixtures + 8 field samples = n = 38.

We analysed all three natural char endmembers and six of the eight naturally occurring field sample char layers (two of the eight had insufficient sample mass remaining) for C, H, N and O using a Costech 4010 Elemental Analyzer calibrated to atropine standard. The values presented reflect the elemental composition of these samples as mixtures of char and peat. The elemental composition is intermediate between condensed hydrocarbon and lignin-like biomolecules (Kim *et al.* 2003), and between high and low temperature chars (Sekiguchi *et al.* 1983), which reflects the products of smouldering combustion in a peat matrix (Figure 1). These values are similar to those of macroscopic char particles
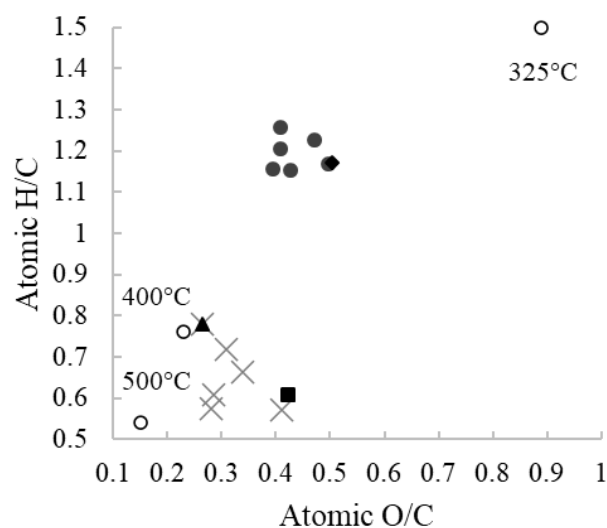


Figure 1. The van Krevelen diagram for nine of the eleven natural char samples used to fit our models. Grey circles are natural char layers, and the black symbols represent the three char endmembers used in making the admixtures. The diamond is the Michigan char, the triangle is the Minnesota char, and the square is the Canadian char. Grey crosses are macroscopic char particles found in the mineral/organic soil interface of boreal spruce forest sites in interior Alaska (Kane *et al.* 2007). Open circles are cellulosic chars produced at the stated temperatures (Sekiguchi *et al.* 1983). Both Kane and Sekiguchi chars are included for reference purposes; see also Table A1 in the Appendix.

found in the mineral/organic soil interface of boreal spruce forest sites in interior Alaska (Kane *et al.* 2007).

**FTIR spectra handling**
We prepared all samples for FTIR by mixing with FTIR-grade KBr to 10 % sample by mass. We mixed samples using a small agate mortar and pestle to further break down the KBr crystals and mix them with the sample. We dried samples at 60 °C for > 24 hours before measuring them with diffuse reflectance FTIR (DRIFT) using a Thermo Scientific Nicolet iS5 spectrometer, equipped with a standard fast recovery deuterated triglycine sulfate (DTGS) detector and an iD Foundation - Diffuse accessory (Thermo Fisher Scientific, Ann Arbor, MI). We chose the DRIFT method due to the ease of sample preparation and its effectiveness on heterogenous samples such as peat (Niemeyer *et al.* 1992). The DRIFT method allows the beam to contact more of the sample than attenuated total reflectance (ATR), which is beneficial for increasing the probability of detecting PyC particles. The DRIFT method is also easily

compatible with current FTIR database efforts such as the USDA-funded SoilSpec4GG initiative (https://soilspectroscopy.org/). We produced spectra of the 400–4000 cm$^{-1}$ range with resolution of 4 cm$^{-1}$ and a data interval of 0.5 cm$^{-1}$ by averaging 64 scans. We used ultrapure N$_2$ purge to further reduce the interference of humidity and to improve spectral fidelity. Automatic background correction built into the software further eliminated remaining atmospheric effects. We acquired background spectra by scanning KBr blank samples at least once every two hours when running samples, to account for changing atmospheric ([CO$_2$], relative humidity) conditions.

We used custom code written in Python to baseline correct and standardise the spectra to compare relative peak areas, rather than absolute data which were variable due to sample properties, dilution factors and atmospheric conditions during testing. Recognising that peaks often overlap, we used the peak fitting function in Origin (Origin 2019b 64-bit, OriginLab Corporation, Northampton, MA) to condense the volume of data per sample by fitting 15 Gaussian peaks to the spectral features, summarising those peak areas for use in modelling. This is an elaboration of the peak derivative measurement methods used by Pandey & Pitman (2003). Whereas that method measures peaks by drawing a line connecting the "bottom" side of each peak and integrating the area between the line and the peak, in contrast, peak fitting allows overlapping of peaks. Identification of overlapping peaks has been flagged as particularly important (see Heller *et al.* 2015) in the densely packed "fingerprint region" of the spectra (850–1875 cm$^{-1}$). Peak fitting also reduces the number of factors that must be considered in model building, allowing more parsimonious statistical methods to be used.

Peak fitting has been used to good effect for FTIR in multiple applications (Zhang *et al.* 2013, Gaffney *et al.* 2015, Belton *et al.* 2018, Gardegaront *et al.* 2018, Sadat & Joye 2020). Reggente *et al.* (2019) have also shown excellent agreement between peak fitting and partial least squares models for FTIR data on atmospheric aerosols. We achieved stability by carefully controlling both the number of peaks to fit and the allowed range of variation in peak location, area and width. This limitation ensured repeatability and stability but sacrificed perfect line fitting in the region between 2000 and 3800 cm$^{-1}$ where the shape of the spectrum was skewed with few distinct peaks (Figure 2). The three peak areas fitted in the 2000–800 cm$^{-1}$ region correlated well with their respective peak heights, despite the imperfect line fitting (Figure A1 in the Appendix). The Python script used to baseline correct and standardise the spectra, and the Origin function files used for peak fitting, are available in the Supplementary Material.

## NMR

We used NMR data to ensure accurate PyC estimates for model fitting and to validate our FTIR models (Figure 3). The molecular mixing model developed by Baldock *et al.* (2004) is a widely accepted method of PyC quantification based on NMR spectrometry (Miesel *et al.* 2015, Leifeld *et al.* 2018). We selected the three "pure" char and two "pure" peat admixture endmembers, and a series of eight putative no char to putative high char unknown samples taken from three peat cores harvested from peatlands in the Upper Peninsula of Michigan for NMR analysis. In reality, all eight unknown samples were determined by NMR to contain some amount of naturally produced char (Table A2). $^{13}$C solid state NMR experiments were performed on a Varian Infinity-Plus NMR spectrometer equipped with a 6 mm MAS broadband probe operating at 399.75 MHz for $^1$H to determine the mass fraction of each sample that was composed of PyC. For each sample, both cross polarisation with total sideband suppression (CPTOSS, or CP for brevity) and direct polarisation (DP) were acquired under 6 kHz magic angle spinning. The CP data were acquired with 16,000 scans, a sweep width of 1000 ppm, a contact time of 1.9 ms, an acquisition time of 5.12 ms, and a recycle delay (d1) of 3 s. The DP data were acquired with 3000 scans, a sweep width of 1000 ppm, an acquisition time of 5.12 ms, and a recycle delay (d1) of 100 s using a standard one-pulse experiment with $^1$H decoupling during acquisition. All data were processed with a 100 Hz Gaussian line broadening and baseline correction. The $^{13}$C chemical shifts were referenced against an external standard of adamantane. Background signal subtraction was performed to remove the signal from the rotor for the DP spectra (there was no background signal from the rotor for the CP spectra). We integrated spectral magnitude in 7 frequency ranges (0–45, 45–60, 60–95, 95–110, 110–145, 145–165 and 165–215 ppm) to inform subsequent modelling. These methods followed similar studies of organic soil samples (Smernik *et al.* 2002b; Miesel *et al.* 2015). We determined total organic C and total N content via dry combustion on an elemental analyser (EHS 4010 gas chromatograph, Costech, Valencia, CA). The NMR spectral integrations and C and N results were used to calculate the composition of each sample using the modified Baldock molecular mixing model (Baldock *et al.* 2004). The output of this regression includes a char (PyC) fraction, which we used to validate the accuracy of our FTIR model estimates. The admixture PyC contents were corrected based on the

original mixing ratio and the NMR-determined PyC contents of the admixture endmembers. NMR spectra and molecular mixing models are available as part of the Supplementary Material.

The direct polarisation NMR method requires long recycle delays due to the slow relaxation of $^{13}C$, as opposed to the CP method which uses a much shorter recycle delay since the relaxation is dependent on $^{1}H$ and the relaxation time of $^{1}H$ is much shorter than that of $^{13}C$ (Mao *et al.* 2000). Another advantage

of CP over DP is that the $^{13}C$ signals in CP are enhanced by $^{1}H$ via $^{1}H$-$^{13}C$ dipolar couplings and the enhancement is different for each $^{13}C$ since the dipolar coupling is different for each $^{13}C$; as a result, the $^{13}C$ signals in CP are not quantitative (Smernik *et al.* 2002a). As opposed to CP, DP is a more quantitative method to detect the more condensed PyC, routinely detecting > 90 % of PyC (Skjemstad *et al.* 1999, Baldock & Smernik 2002, Smernik *et al.* 2002b). Both the CP and DP methods have been
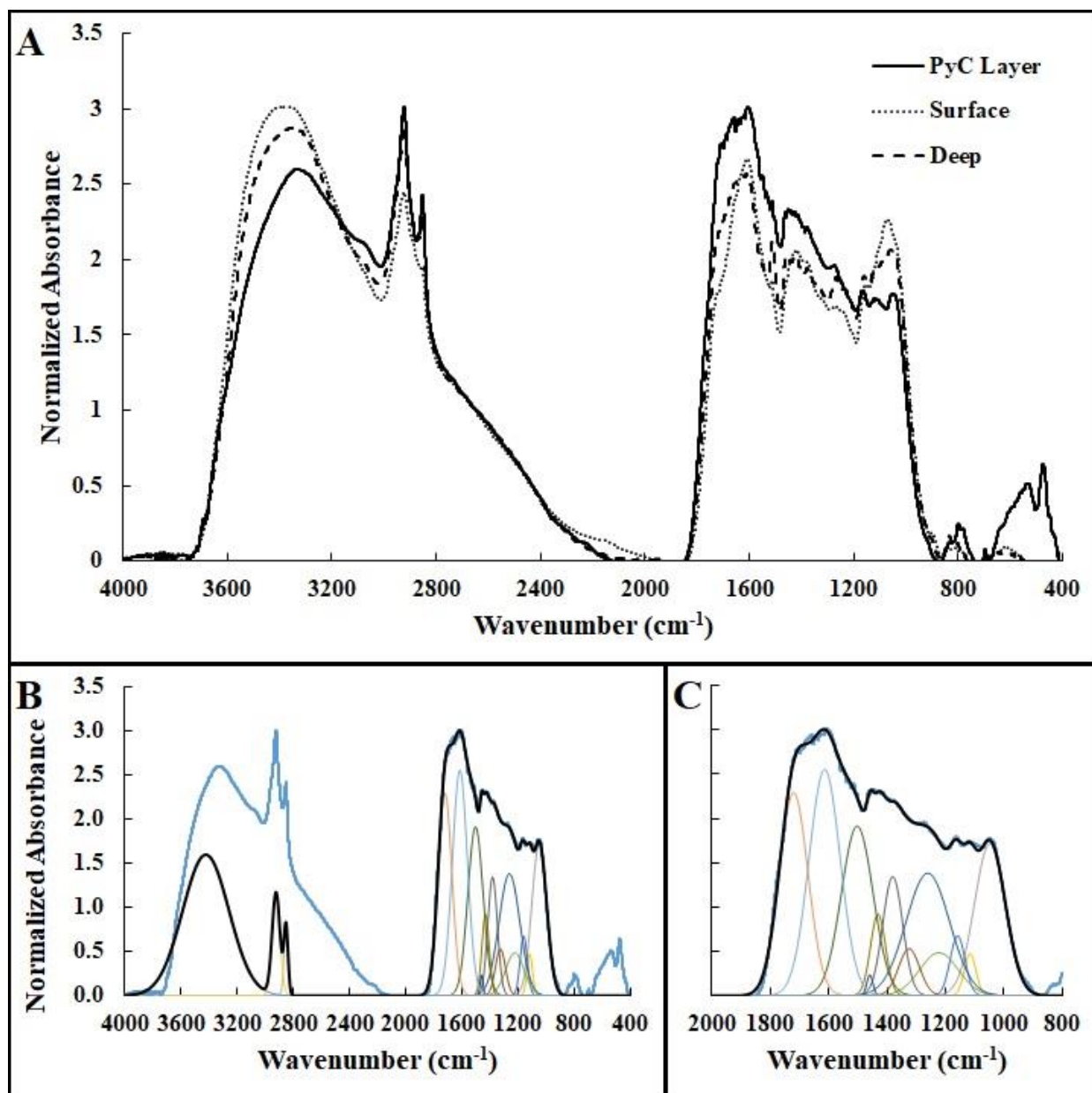


Figure 2. Plot A shows the FTIR spectra of three prototypical samples. The PyC layer is from the Sleeper Lake peatland fire in Michigan, USA. The surface and deep samples are without added PyC; their origins are explained in the admixture preparation subsection of Methods. Plots B and C show the peak fitting results for the PyC sample. Plot B shows the whole spectrum. Plot C shows a detail view of the fingerprint region. In both B and C, the blue line is the original spectrum and the black line is the best fit line built by summing the values of all Gaussian peaks (coloured peaks) fitted to the original.

employed to produce different perspectives on the continuum of PyC, with CP measurements being considered representative of less condensed material and DP measurements representative of more condensed material (Kane *et al.* 2010, Quideau *et al.* 2013). To facilitate this potential use, we evaluated the correlations of both methods to our FTIR data through independent models.

**Model building**

Using the NMR-validated PyC contents for our 30 admixtures and eight field samples, (n=38), we fitted six final linear models and one partial least squares regression (PLSR) model. Peak fitting followed by linear modelling has been used for predicting soil and peat properties (Hodgkins *et al.* 2018, Wilson *et al.*



Figure 3. A comparison of direct polarisation NMR spectra representing three endmembers, surficial *Sphagnum* peat, deep *Sphagnum* peat, and pyrogenic carbon for illustrative purposes.

2022). Partial least squares regression has also been used in similar approaches focused on different soil types (Cotrufo *et al.* 2016, De la Rosa *et al.* 2019, Cadd *et al.* 2020, Sanderman *et al.* 2020). We wanted to apply and compare both methods for predicting PyC in peat. The six linear models predict either DP or CP NMR estimates, and integrate either all matrices (n=38), only surface peat matrices (depth interval 0–40 cm, n=15, surface admixtures only), or only deep peat matrices (depths > 40 cm, n=23, deep admixtures + field samples). The seventh model developed in this study uses PLSR to predict DP NMR estimates in all matrices (n=38). All models were built and tested in JMP (JMP Pro 15, *SAS,* Cary, NC).

Initial linear modelling attempts indicated heteroscedasticity within the data, so a base 10 logarithmic transformation with an offset of 1 to allow the inclusion of 0 values was applied to our known PyC values given by NMR. We used mixed direction, stepwise parameter selection to determine the peaks of greatest statistical importance for predicting PyC. The selected parameters were fitted to the data using standard least squares regression. We used variance inflation factors (VIFs) to eliminate parameters that exhibited multicollinearity. We used PRESS statistics to evaluate a model's suitability for prediction by testing the model accuracy using leave-one-out cross-validation. Having PRESS values similar to their corresponding normal values indicates that the model is not likely overfit to the training data.

We present only one PLSR model because we consider DP NMR predictions the most reliable and the act of subsetting for depth specific models would further limit n, increasing the risk of overfitting. For this modelling approach we used untransformed PyC concentration data as normality is not a requirement of PLSR (Wold *et al.* 2001). Instead, we smoothed the spectra by taking a 5-sample moving average of the absorbances, and then we took the first derivative of those smoothed spectra. We attempted PLSR on pre-smoothed, smoothed, and smoothed first derivative spectra and found the best results using the smoothed first derivative. We also truncated the spectra to between 3980 and 550 cm$^{-1}$ to minimise the ends of the spectra we considered uninformative. We used the NIPALS method (Wold *et al.* 1984) and leave-one-out cross validation. We selected the most parsimonious model, composed of four factors, which did not differ significantly (as determined by Van der Voet T$^2$) from the optimal model (as determined by minimum root mean PRESS), which was composed of seven factors. We also considered the Q$^2$ values which agreed with the above.
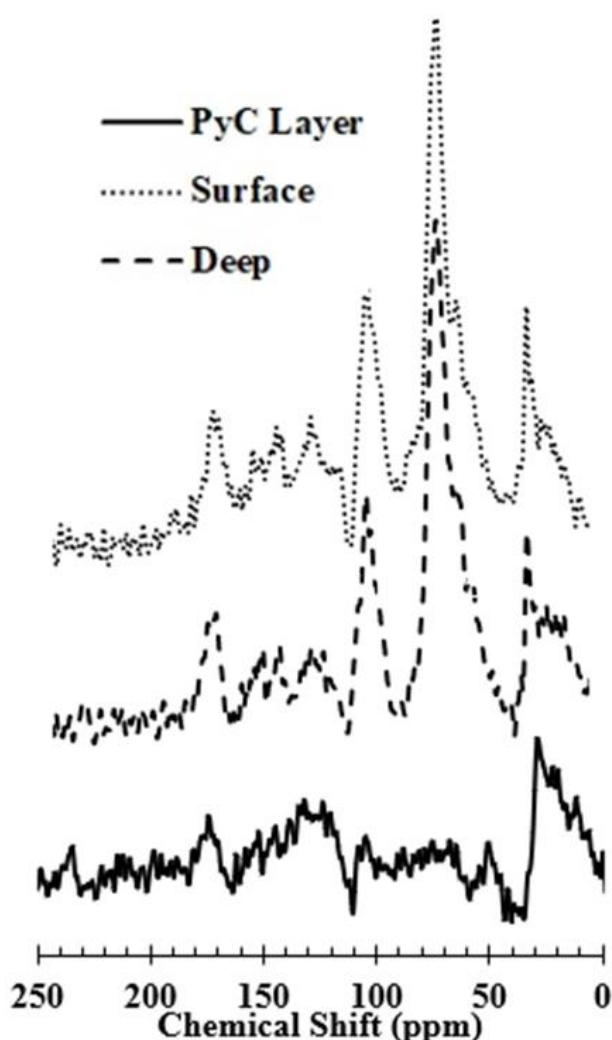
## RESULTS

Elemental analysis (Figure 1) showed that the char endmembers we picked are comparable in condensation to other examples of natural char from similar ecosystems (Kane *et al.* 2007). The natural char layers were generally less condensed than these chars (with the exception of the Michigan Char endmember), which makes sense considering that these natural layers are diluted with uncharred peat matter. The van Krevelen diagram indicates that our samples fall within the expected range in comparison to other examples of similar materials (chars and peat DOM) (Sekiguchi *et al.* 1983, Kane *et al.* 2007, Herzsprung *et al.* 2017, Uhelski & Miesel 2017).

Direct Polarisation NMR measures were consistently higher than CP NMR measures of PyC (Tables A2–A4), which reflects the bias exhibited by CP NMR toward the less condensed moieties discussed above. For this reason, we generally preferred the DP predicting models and we consider this difference to be the primary driver of the difference in quality between the DP and CP predicting models.

The depth-specific linear models explained more of the variance and had better PRESS statistics than the generalised models, particularly the surface specific models, and the greatest differences occurred in the CP predicting models (Table 1 and Figure 4). However, the majority of peat in these particular ecosystems is deep peat, the specific models for which differed little from the overall models. We therefore focus on the two overall models correlating FTIR spectra with NMR measures of peat PyC content, one for DP NMR and one for CP NMR. Using overall models allows us to focus on the

models with the highest n and removes the need to differentiate between deep and surface peat, a boundary that can be difficult to locate in practice, simplifying potential future application. The overall DP predicting model had similar or better PRESS values to depth-specific models predicting DP; given the difference in matrix composition this is remarkable (Table 1). In comparison, the CP predicting overall model was similar in PRESS statistics to the deep peat-specific model but explained less of the variance than the surface peat-specific model (Table 1).

The PLSR DP predicting model (n=38) produces initially impressive results, with four factors explaining over 97 % of the variance in PyC predictions, and almost 60 % of the variance in the spectra (Table 2). However, the $Q^2$ values, which correspond to the linear models PRESS $R^2$ values, are actually lower for the selected PLSR model than for the equivalent linear model. Additionally, the difference between basic correlation values ($R^2$ and cumulative $R^2Y$) and validation correlation values (PRESS $R^2$ and $Q^2$) should ideally be minimal, as the basic correlation values can be easily inflated by some degree of overfitting, while overfitting tends to decrease the validation values.

Both DP and CP models tended to overestimate PyC when PyC concentration was low and to underestimate it when PyC concentration was high (Figure 5). The DP model positively correlated PyC mass fraction with Peak 12 (mean peak location ± standard deviation) (1720 cm$^{-1}$ ± < 0.01) and Peak 3 (1160 cm$^{-1}$ ± 1). These peaks are associated with a wide variety of organic moieties, notably aromatics for Peak 3 and anhydrides for Peak 12 (Table A5). The DP model negatively correlated PyC mass

Table 1. Summary data for direct polarisation and cross polarisation peak fitting MLR models incorporating different depth intervals (0–40 cm, > 40 cm). The models predict the mass percent of PyC in a sample on the log 10 scale, therefore RMSE values are given in the log 10 transformed scale. **Bold** type indicates the overall models that are the focus of analysis. DP refers to direct polarisation and CP refers to cross polarisation, both of which are methods for pyrogenic carbon validation.

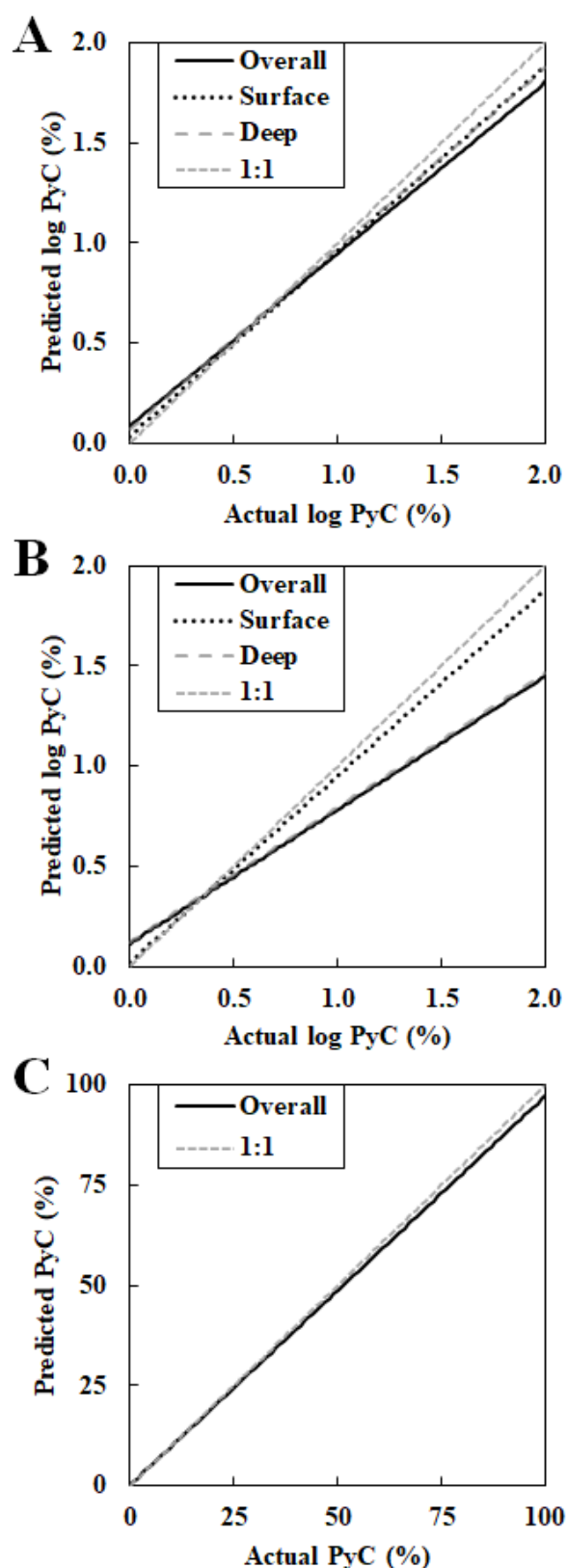| MODEL DATA | | STANDARD TERMS | | | | PRESS STATS | |
|---|---|---|---|---|---|---|---|
| Matrix | Predicting | n | $R^2$ | Adj. $R^2$ | RMSE | PRESS RMSE | PRESS $R^2$ |
| **Overall** | **DP** | **38** | **0.857** | **0.840** | **0.180** | **0.198** | **0.801** |
| Surface | DP | 15 | 0.924 | 0.904 | 0.121 | 0.208 | 0.693 |
| Deep | DP | 23 | 0.902 | 0.880 | 0.163 | 0.204 | 0.802 |
| **Overall** | **CP** | **38** | **0.667** | **0.627** | **0.239** | **0.271** | **0.508** |
| Surface | CP | 15 | 0.929 | 0.909 | 0.114 | 0.157 | 0.813 |
| Deep | CP | 23 | 0.672 | 0.599 | 0.257 | 0.305 | 0.409 |

7

Figure 4. Plots showing predicted versus actual slopes of all models on the log scale, with the 1:1 (y = x) line in dotted grey, for the peak fitted (A) direct polarisation, (B) cross polarisation and (C) PLS direct polarisation models. Model statistics are as presented in Table 2.

fraction with two other peaks, Peak 14 (2921 ± 2) and Peak 7 (1381 ± 0.02). These peaks correlated with other, mostly non-aromatic, organic moieties not strongly associated with PyC (Table 3). The predictive equation for this model is:

$$Y = 0.0682596 + (P3 * 0.0189366) - (P7 * 0.018202) + (P12 * 0.0126316) - (P14 * 0.011629) \quad [1]$$

The CP model positively correlated PyC mass fraction with the same two peaks, 12 (1720 cm$^{-1}$ ± < 0.01) and 3 (1160 cm$^{-1}$ ± 1) (Peak 3 associated notably with aromatics and Peak 12 with anhydrides). It negatively correlated PyC mass fraction with two other peaks, Peak 4 (1229 ± 2.77 cm$^{-1}$) and Peak 7 (1381 ± 0.02 cm$^{-1}$). These peaks were related to other, mostly non-aromatic organic moieties not strongly associated with PyC (Table 3). The predictive model for this is reflected in Equation 2:

$$Y = 0.5919393 + (P3 * 0.0318442) - (P4 * 0.00305) - (P7 * 0.022012) + (P12 * 0.0081828) \quad [2]$$

In Equations 1 and 2, predicted sample PyC mass percent equals $10^{Y+1}$, and PX refers to the area under the peak with the given identification number.

The PLSR model, which integrates almost the entire spectrum, cannot be simplified to a single equation. Ultimately, the particular features considered by the PLSR model are obfuscated by the scale and complexity of the data available in the spectra. This obfuscation by complexity is one detriment of the PLSR approach.

## DISCUSSION

### Model components

We showed that FTIR can be used to make useful predictions of the PyC content of peat soil. The aromatic structures of char may not interact as strongly with infrared light as other, more polar non-char moieties, but we were still able to predict the char content of peat samples with accuracy (Tables 1 and 2). Ultimately, model associations were chosen statistically rather than *a priori* based on their actual correlation in our sample set with the PyC concentrations of eleven different naturally produced peatland chars.

Both the linear DP and CP models correlated positively with Peaks 3 and 12. Peak 3 is associated with C-O and R-O-R bonds (Skoog 2014), and with -C-OH bonds (Niemeyer *et al.* 1992), although contributions may also come from aromatic moieties (Colthup 1950), which are common in PyC. Colthup

Table 2. Summary data for direct polarisation PLS models incorporating different depth intervals (0–40 cm, >40 cm). The models predict the mass percent of PyC in a sample. **Bold** type identifies the model that is the focus of analysis. *Italicised* cells indicate significant (p < 0.05) differences in van der Voet $T^2$.

| Factors | Root Mean PRESS | Prob > van der Voet $T^2$ | $Q^2$ | Cumulative $R^2X$ | Cumulative $R^2Y$ |
|---|---|---|---|---|---|
| 0 | 1.027 | *<.0001* | -0.055 | 0.000 | 0.000 |
| 1 | 0.688 | *<.0001* | 0.526 | 0.297 | 0.643 |
| 2 | 0.629 | *<.0001* | 0.605 | 0.433 | 0.818 |
| 3 | 0.579 | *0.009* | 0.665 | 0.540 | 0.907 |
| **4** | **0.496** | **0.123** | **0.754** | **0.598** | **0.972** |
| 5 | 0.473 | 0.098 | 0.776 | 0.667 | 0.988 |
| 6 | 0.451 | 0.393 | 0.796 | 0.702 | 0.995 |
| 7 | 0.445 | 1.000 | 0.802 | 0.738 | 0.998 |

(1950) associates the region around Peak 12 with anhydrides, a class of molecules which can be formed through pyrolysis of cellulose and hemicellulose (Simoneit *et al.* 1999, Nolte *et al.* 2001). Another possibility is that the Peak 12 signal represents aged PyC, which becomes "enriched in oxygen-containing functional groups such as carboxylic acid, **esters, aldehydes and ketones**" [emphasis added], eventually causing reversion of PyC to humic organic matter or mineralisation (Preston & Schmidt 2006). The latter three moieties are all represented under Peak 12, and could explain its strong relationship to PyC, particularly to aged PyC. Whether this results in overrepresentation of PyC that is older or was more oxidised is unclear and warrants further study.

Both linear models negatively correlated PyC with peaks representing more common moieties, particularly alkanes. It is likely that the negative relationship of our models with alkanes and other uncondensed moieties has less to do with these moieties being unable to coexist with PyC, and more to do with the fact that the predictions are measured in mass fraction. Therefore, any increase in the mass percent contribution from other moieties must result in a decrease in percent PyC. These other moieties represent other constituents of peat including aliphatics, lignin, cellulose and others, with which PyC, if present, must share space.

**Comparison of peak fitting and partial least squares approaches**

Spectral predictive modelling is best suited for large datasets. Spectra are composed of thousands of absorbance values at given wavenumbers, each of which could be treated as highly autocorrelated independent variables (Xs), and we want to use spectra to predict few dependent variables (Ys) (soil properties, such as [PyC]), which is problematic when power (n) is low. The two methods, peak fitting and PLSR, approach this in different ways. Peak fitting reduces the number of Xs and the autocorrelation by summarising the spectral features, condensing them to manageable and interpretable features. The purpose of PLSR for spectral interpretation is to ingest as much of the available spectral data as possible to make the most accurate predictions. In effect, PLSR summarises the spectra into a smaller number of Xs by using what is effectively internal principal components analysis. Each factor is one principal component. However, the PLSR method remains far more difficult to mechanistically interpret than the linear models. While both approaches summarise spectra, the peak fitting approach produces peak areas that directly relate to spectral features which have been thoroughly described. In contrast, each of the four factors in our PLSR model responds uniquely to each observation of absorbance. Even VIP and coefficients plots which summarise the four factors into one single dimension are difficult to interpret due to rapid fluctuations and noise.

Furthermore, PLSR, while relatively transparent and robust to overfitting in comparison to other big data methods such as machine learning, is still a data intense method. Like other studies applying PLSR to PyC, our n was severely limited by the expense of NMR validation (Cotrufo *et al.* 2016, Cadd *et al.* 2020). The amount of variance that can be included in a small dataset such as ours is necessarily limited compared to a properly constructed dataset of a larger n. Pearson *et al.* (2014) recommend >120 calibration samples. Datasets of lower n can more easily lead to overfit models. This is probably why our PLSR model produces far superior $R^2$ compared to the peak

Figure 5 (right). A plot showing predicted versus actual values for the peak fitted (A) overall direct polarisation, (B) overall cross polarisation, and (C) PLS overall direct polarisation models. Depicted are sample points, mean (solid black line), confidence interval (dark grey zone), prediction interval (light grey zone), and 1:1 (y = x) line (dotted grey line). Filled symbols are deep samples, open symbols are surface samples. Squares are Canadian char admixtures, triangles are Minnesota char admixtures, circles are Michigan char admixtures, and diamonds are NMR-validated natural char layers.



fitting linear models but falls flat when validation methods come into play, which reveals that the predictive ability is in fact worse (comparing $Q^2$ to PRESS $R^2$).

Beyond the fact that our PLSR model shows signs of overfitting, there is also the matter of generalisability. It takes a massive database of spectra, reliable soil properties data and metadata to produce spectrometry-based PLSR models which can reliably be applied to landscapes (see, for example, Sanderman *et al.* 2020, 2021), which currently does not exist for organic soils (Histosols). Partial least squares regression can be highly sensitive to attributes unique to individual instruments and calibration transfer, while possible, is difficult (Feudale *et al.* 2002, Workman 2018). Therefore, the application of our PLSR model is limited. Our PLSR model and dataset provide just one step towards a potential future Histosol calibration. As such, for quantification of PyC in peat soil at this time we recommend the peak fitting approach.

**Model application**

For determination of historical fire regimes of peat soil profiles, any FTIR method must be applied to subsamples taken at small enough depth intervals to capture PyC layers with minimal dilution by unaltered peat. We recommend depth intervals of around 2 cm for low bulk density and unfrozen matrices like peat (compared with 0.5–3 cm for sediments; Hoecker *et al.* 2020). Changes in the pattern of burning with fuel type (surficial vegetation versus peat burning) or wildfire intensity may lead to no detectable PyC layer being produced, either due to most C being combusted rather than pyrolysed, or due to little C being affected. Such a scenario is unlikely in a peat wildfire but may be possible in a vegetation fire where fuel can be finer and drier, and thus more susceptible to flaming as opposed to smouldering. The threshold for detectability largely
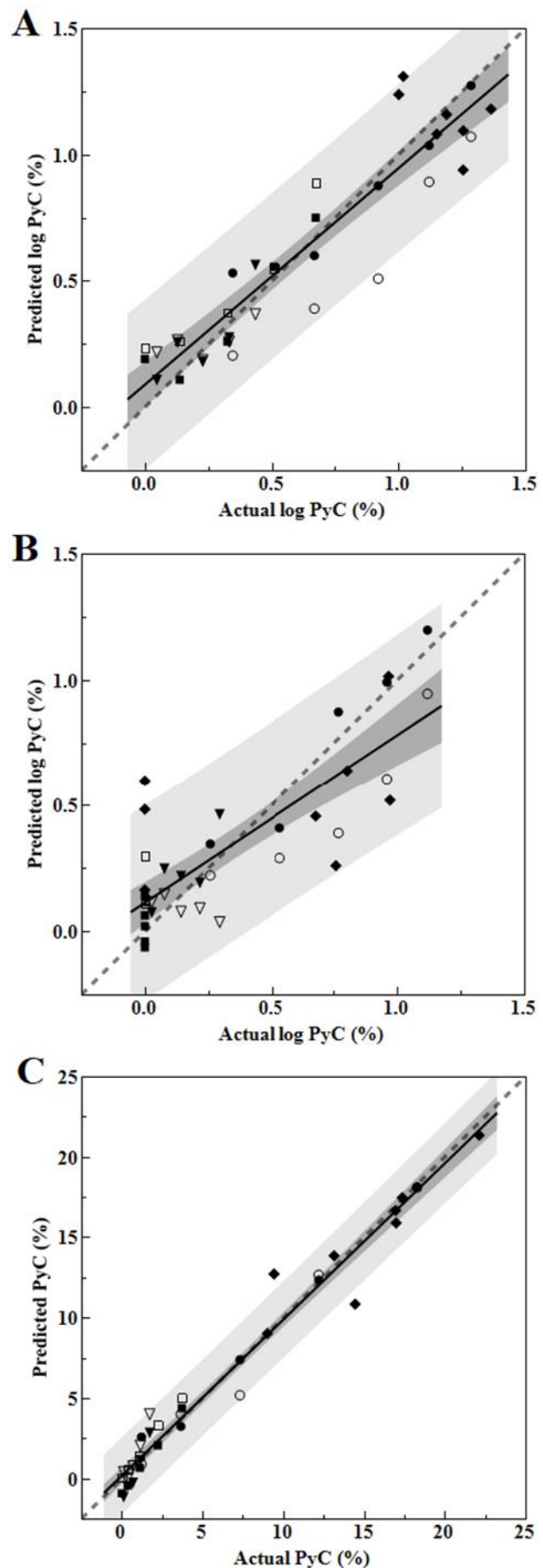
depends on the thickness of each sample and the calibration of the model. Layers of PyC may overlap one another, or an antecedent layer could be consumed by one or more succeeding fires, so estimates of fire regimes must consider these complications. Moreover, in wetlands with lateral flow (such as fens), recent PyC may simply be translocated (cf., Masiello & Berhe 2020), but this is less likely in more ombrotrophic peatlands. We suggest that PyC layers could be distinguished when a spike in predicted PyC exists within the profile, deviating from a baseline minimum PyC content determined by the model user. If a PyC layer is thick enough, or if there is vertical movement of PyC, multiple subsamples could be affected in a vertical sequence, so we recommend that PyC spikes in the profile be counted rather than individual subsamples composing the spike, to avoid overestimating fire occurrence. Using these methods and keeping in mind these considerations should help produce conservative minimum fire return intervals for a given peat profile. These techniques in combination with radiocarbon dating should be useful tools in deriving minimum fire frequencies or maximum average fire return intervals in peatlands.

**Model limitations**

While the models utilised here show promise for evaluating the fire histories of peatlands, they were fitted to a limited range of real PyC contents, so may not accurately predict samples exceeding this range. Additionally, it has recently been shown that the spectral properties of PyC produced at high temperatures are significantly different from those of PyC produced at lower temperatures (Gao *et al.* 2022). As such, burn conditions including temperature and duration can influence the PyC signal to some degree. The FTIR spectra recorded from peat will be a product of both the contents of the peat and their relative abundances, so we cannot precisely discern whether spectral features are due to PyC characteristics or PyC abundance without isolation of the PyC. Notwithstanding, we highlight here that our models reliably identified natural PyC with likely variable burn conditions and time since fire, which suggests our models are at least somewhat robust to fire condition variance within this ecosystem type. We chose this approach over one including "pure" graphitic PyC because this would not be representative of natural chars, particularly in peatlands. We fitted our models on peat representative of *Sphagnum*-dominated northern peatlands, so different peat sources (and changes in burn conditions) may reduce the accuracy of the models in other ecosystems. However, the peaks used

in each peak fitting model are related to moieties present in a broad range of peat types (cf., Hodgkins *et al.* 2018), suggesting these models may be broadly applicable within this ecosystem type. Applying this type of model would require accepting the assumptions that the peat and char being measured fall within the range of variation of the samples used to fit this model. In which case, the PRESS statistics for the models would give the best indication of the appropriate level of certainty. Therefore, we recommend validation measures be taken for individual studies, particularly on peats that are significantly different, such as those from tropical peatlands. We invite further study to validate the peak fitting method and to contribute to broadening the peat, char and instrumental datasets necessary to make broadly applicable PLSR models of peat soil properties for the research community to use.

## ACKNOWLEDGEMENTS

## AUTHOR CONTRIBUTIONS

DU, KH, EK and RC developed the methods. DU and KH led the FTIR laboratory analysis. JM and LX led the NMR laboratory analysis. DU wrote the manuscript. DU, EK, RC, KH, JM and LX contributed to editing the manuscript.

## REFERENCES

Artz, R.R.E., Chapman, S.J., Campbell, C.D. (2006) Substrate utilisation profiles of microbial communities in peat are depth dependent and correlate with whole soil FTIR profiles. *Soil Biology and Biochemistry*, 38(9), 2958–2962. doi: 10.1016/j.soilbio.2006.04.017.

Artz, R.R.E., Chapman, S.J., Jean Robertson, A.H., Potts, J.M., Laggoun-Défarge, F., Gogo, S., Comont, L., Disnar, J.R., Francez, A.J. (2008) FTIR spectroscopy can be used as a screening tool

for organic matter quality in regenerating cutover peatlands. *Soil Biology and Biochemistry*, 40(2), 515–527. doi: 10.1016/j.soilbio.2007.09.019.

Ashby, M.A., Heinemeyer, A. (2021) A critical review of the IUCN UK Peatland Programme's "Burning and Peatlands" position statement. *Wetlands*, 41(5), 56, 22 pp. doi: 10.1007/s13157-021-01400-1.

Baldock, J.A., Smernik, R.J. (2002) Chemical composition and bioavailability of thermally altered *Pinus resinosa* (Red pine) wood. *Organic Geochemistry*, 33(9), 1093–1109. doi: 10.1016/S0146-6380(02)00062-1.

Baldock, J.A., Masiello, C.A., Gélinas, Y., Hedges, J.I. (2004) Cycling and composition of organic matter in terrestrial and marine ecosystems. *Marine Chemistry*, 92(1–4), 39–64. doi: 10.1016/j.marchem.2004.06.016.

Belton, D.J., Plowright, R., Kaplan, D.L., Perry, C.C. (2018) A robust spectroscopic method for the determination of protein conformational composition - Application to the annealing of silk. *Acta Biomaterialia*, 73, 355–364. doi: 10.1016/j.actbio.2018.03.058.

Benscoter, B.W., Greenacre, D., Turetsky, M.R. (2015) Wildfire as a key determinant of peatland microtopography. *Canadian Journal of Forest Research*, 45, 1133–1137. doi: 10.1139/cjfr-2015-0028.

Bess, J.A., Chimner, R.A., Kangas, L.C. (2014) Ditch restoration in a large Northern Michigan fen: Vegetation response and basic porewater chemistry. *Ecological Restoration*, 32(3), 260–274. doi: 10.3368/ER.32.3.260.

Bourgeau-Chavez, L.L., Grelik, S.L., Billmire, M., Jenkins, L.K., Kasischke, E.S., Turetsky, M.R. (2020) Assessing boreal peat fire severity and vulnerability of peatlands to early season wildland fire. *Frontiers in Forests and Global Change*, 3, 20, 13 pp. doi: 10.3389/ffgc.2020.00020.

Cadd, H.R., Tyler, J., Tibby, J., Baldock, J., Hawke, B., Barr, C., Leng, M.J. (2020) The potential for rapid determination of charcoal from wetland sediments using infrared spectroscopy. *Palaeogeography, Palaeoclimatology, Palaeoecology*, 542, 109562, 13 pp. doi: 10.1016/j.palaeo.2019.109562.

Chen, J., Gu, B., LeBoeuf, E.J., Pan, H., Dai, S. (2002) Spectroscopic characterization of the structural and functional properties of natural organic matter fractions. *Chemosphere*, 48(1), 59–68. doi: 10.1016/S0045-6535(02)00041-3.

Chimner, R.A., Ott, C.A., Perry, C.H., Kolka, R.K. (2014) Developing and evaluating rapid field methods to estimate peat carbon. *Wetlands*, 34(6),

1241–1246. doi: 10.1007/s13157-014-0574-6.

Clark, J.S., Hussey, T.C. (1996) Estimating the mass flux of charcoal from sedimentary records: effects of particle size, morphology, and orientation. *The Holocene*, 6(2), 129–144. doi: 10.1177/095968369600600201.

Cocozza, C., D'Orazio, V., Miano, T.M., Shotyk, W. (2003) Characterization of solid and aqueous phases of a peat bog profile using molecular fluorescence spectroscopy, ESR and FT-IR, and comparison with physical properties. *Organic Geochemistry*, 34, 49–60. doi: 10.1016/S0146-6380(02)00208-5.

Colthup, N.B. (1950) Spectra-structure correlations in the infra-red region. *Journal of the Optical Society of America*, 40(6), 397–400. doi: 10.1364/JOSA.40.000397

Cotrufo, M.F., Boot, C., Abiven, S., Foster, E.J., Haddix, M., Reisser, M., Wurster, C.M., Bird, M.I., Schmidt, M.W.I. (2016) Quantification of pyrogenic carbon in the environment: An integration of analytical approaches. *Organic Geochemistry*, 100, 42–50. doi: 10.1016/j.orggeochem.2016.07.007.

Crausbay, S.D., Higuera, P.E., Sprugel, D.G., Brubaker, L.B. (2017) Fire catalyzed rapid ecological change in lowland coniferous forests of the Pacific Northwest over the past 14,000 years. *Ecology*, 98(9), 2356–2369. doi: 10.1002/ecy.1897.

De la Rosa, J.M., Jiménez-González, M.A., Jiménez-Morillo, N.T., Knicker, H., Almendros, G. (2019) Quantitative forecasting black (pyrogenic) carbon in soils by chemometric analysis of infrared spectra. *Journal of Environmental Management*, 251, 109567, 8 pp. doi: 10.1016/j.jenvman.2019.109567.

Demyan, M.S., Rasche, F., Schulz, E., Breulmann, M., Müller, T., Cadisch, G. (2012) Use of specific peaks obtained by diffuse reflectance Fourier transform mid-infrared spectroscopy to study the composition of organic matter in a Haplic Chernozem. *European Journal of Soil Science*, 63(2), 189–199. doi: 10.1111/j.1365-2389.2011.01420.x.

Ding, G., Rice, J.A. (2012) Black carbon evaluation in natural organic matter samples using recoupled long-range dipolar dephasing solid-state $^{13}$C NMR. *Geoderma*, 189–190, 381–387. doi: 10.1016/j.geoderma.2012.04.020.

Farage, P., Ball, A., McGenity, T.J., Whitby, C., Pretty, J. (2009) Burning management and carbon sequestration of upland heather moorland in the UK. *Australian Journal of Soil Research*, 47(4), 351–361. doi: 10.1071/SR08095.

Feudale, R.N., Woody, N.A., Tan, H., Myles, A.J.,

12

Brown, S.D., Ferré, J. (2002) Transfer of multivariate calibration models: A review. *Chemometrics and Intelligent Laboratory Systems*, 64(2), 181–192. doi: 10.1016/S0169-7439(02)00085-0.

Gaffney, J.S., Marley, N.A., Smith, K.J. (2015) Characterization of fine mode atmospheric aerosols by Raman microscopy and diffuse reflectance FTIR. *Journal of Physical Chemistry A*, 119(19), 4524–4532. doi: 10.1021/jp510361s.

Gałka, M., Miotk-Szpiganowicz, G., Marczewska, M., Barabach, J., van der Knaap, W.O., Lamentowicz, M. (2015) Palaeoenvironmental changes in Central Europe (NE Poland) during the last 6200 years reconstructed from a high-resolution multi-proxy peat archive. *The Holocene*, 25(3), 421–434. doi: 10.1177/0959683614561887.

Gao, C., Cong, J., Sun, Y., Han, D., Wang, G. (2022) Variability in pyrogenic carbon properties generated by different burning temperatures and peatland plant litters: implication for identifying fire intensity and fuel types. *International Journal of Wildland Fire*, 213–327. doi: 10.1071/wf21053.

Gardegaront, M., Farlay, D., Peyruchaud, O., Follet, H. (2018) Automation of the peak fitting method in bone FTIR microspectroscopy spectrum analysis: Human and mice bone study. *Journal of Spectroscopy*, 2018, 4131029, 11 pp. doi: 10.1155/2018/4131029.

Goldberg, E.D. (1985) *Black Carbon in the Environment: Properties and Distribution*. John Wiley and Sons, New York, 198 pp.

Goldstein, A., Turner, W.R., Spawn, S.A., Anderson-Teixeira, K.J., Cook-Patton, S., Fargione, J., Gibbs, H.K., Griscom, B., Hewson, J.H., Howard, J.F., Ledezma, J.C., Page, S., Koh, L.P., Rockström, J., Sanderman, J., Hole, D.G. (2020) Protecting irrecoverable carbon in Earth's ecosystems. *Nature Climate Change*, 10, 287–295. doi: 10.1038/s41558-020-0738-8.

Guo, Y., Bustin, R.M. (1998) FTIR spectroscopy and reflectance of modern charcoals and fungal decayed woods: implications for studies of inertinite in coals. *International Journal of Coal Geology*, 37(1–2), 29–53. doi: 10.1016/S0166-5162(98)00019-6.

Hammes, K., Schmidt, M.W.I., Smernik, R.J., Currie, L.A. and 38 others (2007) Comparison of quantification methods to measure fire-derived (black-elemental) carbon in soils and sediments using reference materials from soil, water, sediment and the atmosphere. *Global Biogeochemical Cycles*, 21(3), GB3016, 18 pp. doi: 10.1029/2006GB002914.

Hardy, B., Leifeld, J., Knicker, H., Dufey, J.E.,

Deforce, K., Cornélis, J.T. (2017) Long term change in chemical properties of preindustrial charcoal particles aged in forest and agricultural temperate soil. *Organic Geochemistry*, 107, 33–45. doi: 10.1016/j.orggeochem.2017.02.008.

Harper, A.R., Doerr, S.H., Santin, C., Froyd, C.A., Sinnadurai, P. (2018) Prescribed fire and its impacts on ecosystem services in the UK. *Science of The Total Environment*, 624, 691–703. doi: 10.1016/j.scitotenv.2017.12.161.

Hatten, J.A., Zabowski, D. (2009) Changes in soil organic matter pools and carbon mineralization as influenced by fire severity. *Soil Science Society of America Journal*, 73(1), 262–273. doi: 10.2136/sssaj2007.0304.

Hedges, J.I., Eglinton, G., Hatcher, P.G., Kirchman, D.L., Arnosti, C., Derenne, S., Evershed, R.P., Kögel-Knabner, I., De Leeuw, J.W., Littke, R., Michaelis, W., Rullkötter, J. (2000) The molecularly-uncharacterized component of nonliving organic matter in natural environments. *Organic Geochemistry*, 31(10), 945–958. doi: 10.1016/S0146-6380(00)00096-6.

Heller, C., Ellerbrock, R.H., Roßkopf, N., Klingenfuß, C., Zeitz, J. (2015) Soil organic matter characterization of temperate peatland soil with FTIR-spectroscopy: Effects of mire type and drainage intensity. *European Journal of Soil Science*, 66(5), 847–858. doi: 10.1111/ejss.12279.

Herzsprung, P., Osterloh, K., von Tümpling, W., Harir, M., Hertkorn, N., Schmitt-Kopplin, P., Meissner, R., Bernsdorf, S., Friese, K. (2017) Differences in DOM of rewetted and natural peatlands - Results from high-field FT-ICR-MS and bulk optical parameters. *Science of the Total Environment*, 586, 770–781. doi: 10.1016/j.scitotenv.2017.02.054.

Hodgkins, S.B., Richardson, C.J., Dommain, R., Wang, H. and 19 others (2018) Tropical peatland carbon storage linked to global latitudinal trends in peat recalcitrance. *Nature Communications*, 9(1), 3640, 13 pp. doi: 10.1038/s41467-018-06050-2.

Hoecker, T.J., Higuera, P.E., Kelly, R., Hu, F.S. (2020) Arctic and boreal paleofire records reveal drivers of fire activity and departures from Holocene variability. *Ecology*, 101(9), e03096, 17 pp. doi: 10.1002/ecy.3096.

Kaal, J., Baldock, J.A., Buurman, P., Nierop, K.G.J., Pontevedra-Pombal, X., Martínez-Cortizas, A. (2007) Evaluating pyrolysis-GC/MS and $^{13}$C CPMAS NMR in conjunction with a molecular mixing model of the Penido Vello peat deposit, NW Spain. *Organic Geochemistry*, 38(7), 1097–1111. doi: 10.1016/j.orggeochem.2007.02.008.

13

Kane, E.S., Kasischke, E.S., Valentine, D.W., Turetsky, M.R., McGuire, A.D. (2007) Topographic influences on wildfire consumption of soil organic carbon in interior Alaska: Implications for black carbon accumulation. *Journal of Geophysical Research: Biogeosciences*, 112, G03017, 11 pp. doi: 10.1029/2007JG000458.

Kane, E.S., Hockaday, W.C., Turetsky, M.R., Masiello, C.A., Valentine, D.W., Finney, B.P., Baldock, J.A. (2010) Topographic controls on black carbon accumulation in Alaskan black spruce forest soils: Implications for organic matter dynamics. *Biogeochemistry*, 100(1), 39–56. doi: 10.1007/s10533-009-9403-z.

Kasin, I., Blanck, Y.L., Storaunet, K.O., Rolstad, J., Ohlson, M. (2013) The charcoal record in peat and mineral soil across a boreal landscape and possible linkages to climate change and recent fire history. *The Holocene*, 23(7), 1052–1065. doi: 10.1177/0959683613479678.

Kim, S., Kramer, R.W., Hatcher, P.G. (2003) Graphical method for analysis of ultrahigh-resolution broadband mass spectra of natural organic matter, the van Krevelen diagram. *Analytical Chemistry*, 75(20), 5336–5344. doi: 10.1021/ac034415p.

Knicker, H., Müller, P., Hilscher, A. (2007) How useful is chemical oxidation with dichromate for the determination of "Black Carbon" in fire-affected soils? *Geoderma*, 142(1–2), 178–196. doi: 10.1016/j.geoderma.2007.08.010.

Leifeld, J., Alewell, C., Bader, C., Krüger, J.P., Mueller, C.W., Sommer, M., Steffens, M., Szidat, S. (2018) Pyrogenic carbon contributes substantially to carbon storage in intact and degraded northern peatlands. *Land Degradation and Development*, 29(7), 2082–2091. doi: 10.1002/ldr.2812.

Maestrini, B., Miesel, J.R. (2017) Modification of the weak nitric acid digestion method for the quantification of black carbon in organic matrices. *Organic Geochemistry*, 103, 136–139. doi: 10.1016/j.orggeochem.2016.10.010.

Mao, J.-D., Hu, W.-G., Schmidt-Rohr, K., Davies, G., Ghabbour, E.A., Xing, B. (2000) Quantitative characterization of humic substances by solid-state carbon-13 nuclear magnetic resonance. *Soil Science Society of America Journal*, 64(3), 873–884. doi: 10.2136/sssaj2000.643873x.

Margenot, A.J., Calderón, F.J., Magrini, K.A., Evans, R.J. (2017) Application of DRIFTS, ^{13}C NMR, and py-MBMS to characterize the effects of soil science oxidation assays on soil organic matter composition in a mollic xerofluvent. *Applied Spectroscopy*, 71(7), 1506–1518. doi: 10.1177/0003702817691776.

Markgraf, V., Huber, U.M. (2010) Late and postglacial vegetation and fire history in Southern Patagonia and Tierra del Fuego. *Palaeogeography, Palaeoclimatology, Palaeoecology*, 297(2), 351–366. doi: 10.1016/j.palaeo.2010.08.013.

Masiello, C.A. (2004) New directions in black carbon organic geochemistry. *Marine Chemistry*, 92, 201–213. doi: 10.1016/j.marchem.2004.06.043.

Masiello, C.A., Berhe, A.A. (2020) First interactions with the hydrologic cycle determine pyrogenic carbon's fate in the Earth system. *Earth Surface Processes and Landforms*, 45(10), 2394–2398. doi: 10.1002/ESP.4925.

Matamala, R., Calderón, F.J., Jastrow, J.D., Fan, Z., Hofmann, S.M., Michaelson, G.J., Mishra, U., Ping, C.L. (2017) Influence of site and soil properties on the DRIFT spectra of northern cold-region soils. *Geoderma*, 305, 80–91. doi: 10.1016/j.geoderma.2017.05.014.

Merino, A., Chávez-Vergara, B., Salgado, J., Fonturbel, M.T., García-Oliva, F., Vega, J.A. (2015) Variability in the composition of charred litter generated by wildfire in different ecosystems. *Catena*, 133, 52–63. doi: 10.1016/ j.catena.2015.04.016.

Miesel, J.R., Hockaday, W.C., Kolka, R.K., Townsend, P.A. (2015) Soil organic matter composition and quality across fire severity gradients in coniferous and deciduous forests of the southern boreal region. *Journal of Geophysical Research: Biogeosciences*, 120(6), 1124–1141. doi: 10.1002/2015JG002959.

Nichols, J.E., Peteet, D.M. (2019) Rapid expansion of northern peatlands and doubled estimate of carbon storage. *Nature Geoscience*, 12(11), 917–922. doi: 10.1038/s41561-019-0454-z.

Niemeyer, J., Chen, Y., Bollag, J.-M. (1992) Characterization of humic acids, composts, and peat by Diffuse Reflectance Fourier-Transform Infrared Spectroscopy. *Soil Science Society of America Journal*, 56, 135–140. doi: 10.2136/sssaj1992.03615995005600010021x.

Nocentini, C., Certini, G., Knicker, H., Francioso, O., Rumpel, C. (2010) Nature and reactivity of charcoal produced and added to soil during wildfire are particle-size dependent. *Organic Geochemistry*, 41(7), 682–689. doi: 10.1016/ j.orggeochem.2010.03.010.

Nolte, C.G., Schauer, J.J., Cass, G.R., Simoneit, B.R.T. (2001) Highly polar organic compounds present in wood smoke and in the ambient atmosphere. *Environmental Science and Technology*, 35(10), 1912–1919. doi: 10.1021/ es001420r.

Pandey, K.K., Pitman, A.J. (2003) FTIR studies of

14

the changes in wood chemistry following decay by brown-rot and white-rot fungi. *International Biodeterioration and Biodegradation*, 52(3), 151–160. doi: 10.1016/S0964-8305(03)00052-0.

Pearson, E.J., Juggins, S., Tyler, J. (2014) Ultrahigh resolution total organic carbon analysis using Fourier Transform Near Infrared Reflectance Spectroscopy (FT-NIRS). *Geochemistry, Geophysics, Geosystems*, 15(1), 292–301. doi: 10.1002/2013GC004928.

Potvin, L.R., Kane, E.S., Chimner, R.A., Kolka, R.K., Lilleskov, E.A. (2015) Effects of water table position and plant functional group on plant community, aboveground production, and peat properties in a peatland mesocosm experiment (PEATcosm). *Plant and Soil*, 387(1–2), 277–294. doi: 10.1007/s11104-014-2301-8.

Prasad, M., Verhagen, J.B.G.M., Aendekerk, T.G.L. (2000) Effect of peat type and pH on breakdown of peat using fourier transform infrared spectroscopy. *Communications in Soil Science and Plant Analysis*, 31(17–18), 2881–2889. doi: 10.1080/00103620009370635.

Preston, C.M., Schmidt, M.W.I. (2006) Black (pyrogenic) carbon: a synthesis of current knowledge and uncertainties with special consideration of boreal regions. *Biogeosciences*, 3(C), 397–420. doi: 10.5194/bg-3-397-2006.

Quideau, S.A., Norris, C.E., Soucémarianadin, L.N., Wasylishen, R.E. (2013) Forest ecology and soils. *eMagRes*, 2(4), 597–608. doi: 10.1002/9780470034590.emrstm1339.

Reggente, M., Dillner, A.M., Takahama, S. (2019) Analysis of functional groups in atmospheric aerosols by infrared spectroscopy: Systematic intercomparison of calibration methods for US measurement network samples. *Atmospheric Measurement Techniques*, 12(4), 2287–2312. doi: 10.5194/amt-12-2287-2019.

Sadat, A., Joye, I.J. (2020) Peak fitting applied to Fourier Transform Infrared and Raman spectroscopic analysis of proteins. *Applied Sciences*, 10(17), 5918, 16 pp. doi: 10.3390/ app10175918.

Sanderman, J., Savage, K., Dangal, S.R.S. (2020) Mid-infrared spectroscopy for prediction of soil health indicators in the United States. *Soil Science Society of America Journal*, 84(1), 251–261. doi: 10.1002/saj2.20009.

Sanderman, J., Savage, K., Dangal, S.R.S., Duran, G., Rivard, C., Cavigelli, M.A., Gollany, H.T., Jin, V.L., Liebig, M.A., Omondi, E.C., Rui, Y., Stewart, C. (2021) Can agricultural management induced changes in soil organic carbon be detected using mid-infrared spectroscopy? *Remote Sensing*, 13(12), 1–18. doi: 10.3390/ rs13122265.

Schmidt, M.W.I., Skjemstad, J.O., Czimczik, C.I., Glaser, B., Prentice, K.M., Gelinas, Y., Kuhlbusch, T.A.J. (2001) Comparative analysis of black carbon in soils. *Global Biogeochemical Cycles*, 15(1), 163–167. doi: 10.1029/2000GB001284.

Sekiguchi, Y., Frye, J.S., Shafizadeh, F. (1983) Structure and formation of cellulosic chars. *Journal of Applied Polymer Science*, 28(11), 3513–3525. doi: 10.1002/app.1983.070281116.

Simoneit, B.R.T., Schauer, J.J., Nolte, C.G., Oros, D.R., Elias, V.O., Fraser, M.P., Rogge, W.F., Cass, G.R. (1999) Levoglucosan, a tracer for cellulose in biomass burning and atmospheric particles. *Atmospheric Environment*, 33(2), 173–182. doi: 10.1016/S1352-2310(98)00145-9.

Skjemstad, J.O., Taylor, J.A., Smernik, R.J. (1999) Estimation of charcoal (char) in soils. *Communications in Soil Science and Plant Analysis*, 30(15–16), 2283–2298. doi: 10.1080/ 00103629909370372.

Skoog, D.A. (2014) *Fundamentals of Analytical Chemistry*. Ninth edition, Thomson-Brooks/Cole, Belmont, California, 722–759.

Smernik, R.J., Baldock, J.A., Oades, J.M. (2002a) Impact of remote protonation on $^{13}$C CPMAS NMR quantitation of charred and uncharred wood. *Solid State Nuclear Magnetic Resonance*, 22(1), 71–82. doi: 10.1006/snmr.2002.0065.

Smernik, R.J., Baldock, J.A., Oades, J.M., Whittaker, A.K. (2002b) Determination of T1$\rho$H relaxation rates in charred and uncharred wood and consequences for NMR quantitation. *Solid State Nuclear Magnetic Resonance*, 22(1), 50–70. doi: 10.1006/snmr.2002.0064.

Turetsky, M.R., Benscoter, B., Page, S., Rein, G., van der Werf, G.R., Watts, A. (2015) Global vulnerability of peatlands to fire and carbon loss. *Nature Geoscience*, 8(1), 11–14. doi: 10.1038/ NGEO2325.

Uhelski, D., Miesel, J.R. (2017) Physical location in the tree during forest fire influences element concentrations of bark-derived pyrogenic carbon from charred jack pines (*Pinus banksiana* Lamb.). *Organic Geochemistry*, 110, 87–91. doi: 10.1016/ j.orggeochem.2017.04.014.

Wilson, R.M., Hough, M.A., Verbeke, B.A., Hodgkins, S.B., Tyson, G., Sullivan, M.B., Brodie, E., Riley, W.J., Woodcroft, B., McCalley, C., Dominguez, S.C., Crill, P.M., Varner, R.K., Frolking, S., Cooper, W.T., Chanton, J.P., Saleska, S.D., Rich, V.I., Tfaily, M.M. (2022) Plant organic matter inputs exert a strong control on soil organic matter decomposition in a thawing permafrost peatland. *Science of the Total Environment*, 820, 152757, 13 pp. doi: 10.1016/

15

j.scitotenv.2021.152757.

Wold, S., Ruhe, A., Wold, H., Dunn, W.J.III (1984) The collinearity problem in linear regression. The Partial Least Squares (PLS) approach to generalized inverses. *SIAM Journal on Scientific and Statistical Computing*, 5(3), 735–743. doi: 10.1137/0905052.

Wold, S., Sjöström, M., Eriksson, L. (2001) PLS-regression: A basic tool of chemometrics. *Chemometrics and Intelligent Laboratory Systems*, 58(2), 109–130. doi: 10.1016/S0169-7439(01)00155-1.

Workman, J.J. (2018) A review of calibration transfer practices and instrument differences in spectroscopy. *Applied Spectroscopy*, 72(3), 340–365. doi: 10.1177/0003702817736064.

Zhang, Y., Maxted, J., Barber, A., Lowe, C., Smith, R. (2013) The durability of clear polyurethane coil coatings studied by FTIR peak fitting. *Polymer Degradation and Stability*, 98(2), 527–534. doi: 10.1016/j.polymdegradstab.2012.12.003.

*Submitted 18 Apr 2022, final revision 23 Sep 2022*
*Editor: Olivia Bragg*

---

Author for correspondence: Dominic Uhelski, College of Forest Resources and Environmental Science, Michigan Technological University, U.J. Noblet Forestry Building, 1400 Townsend Drive, Houghton, MI 49931-1295, USA.   E-mail: dmuhelsk@mtu.edu

## SUPPLEMENTARY MATERIAL

The supplementary material for this article is available for separate download as a single .zip file. This material includes the Python script used to baseline correct batches of spectra saved as .CSV files; the OriginPro peak fitting batch processing template file; Excel files containing the details of all seven models produced (PLSR overall, DP overall, shallow, and deep, CP overall, shallow, and deep); more information on the specific samples analysed with ^{13}C NMR; also the NMR and FTIR data.

# Appendix

Table A1. Atomic ratios for the van Krevelen diagram presented in Figure 1.

| Source | Identifier | O/C AtomicR | H/C AtomicR |
|---|---|---|---|
| This study | Field Sample | 0.47 | 1.22 |
| | Field Sample | 0.41 | 1.26 |
| | Field Sample | 0.50 | 1.17 |
| | Field Sample | 0.40 | 1.16 |
| | Field Sample | 0.43 | 1.15 |
| | Field Sample | 0.41 | 1.20 |
| | MIC | 0.50 | 1.17 |
| | CAC | 0.42 | 0.61 |
| | MNC | 0.27 | 0.78 |
| Kane *et al*. (2007) char samples DOI: 10.1029/2007JG000458 | ML1P3 | 0.26 | 0.34 |
| | HM2P2 | 0.29 | 0.61 |
| | MM1P2 | 0.23 | 0.42 |
| | PH3P1 | 0.34 | 0.66 |
| | PH2P4 | 0.31 | 0.72 |
| | MH1P4 | 0.41 | 0.57 |
| | HH3P6 | 0.28 | 0.57 |
| | HH3P5 | 0.26 | 0.78 |
| Sekiguchi *et al*. (1983) samples DOI: 10.1002/app.1983.070281116 | 500 deg C | 0.15 | 0.54 |
| | 400 deg C | 0.23 | 0.76 |
| | 325 deg C | 0.89 | 1.50 |

Table A2. Summary of NMR chemical shift regions and pyrogenic carbon concentration ([PyC]) predicted by the modified molecular mixing model (Baldock *et al.* 2004). Further data are available in Tables A3 and A4.

| | | | | Relative contribution (%) of chemical shift region (ppm) | | | | | | Predicted [PyC] (%) |
| | | | Alkyl C 0–45 | O-Alkyl C | | | Aryl C | | Amide/Carboxyl 165–215 | |
| | | | | N-Alkyl/Methoxyl 45–60 | O-Alkyl 60–95 | Di-O-Alkyl 95–110 | Aromatic 110–145 | Phenolic 145–165 | | |
|---|---|---|---|---|---|---|---|---|---|---|
| Direct polarisation NMR | Endmembers | Surface *Sph* | 16.89 | 8.43 | 34.35 | 12.45 | 12.24 | 6.81 | 8.83 | 0.0 |
| | | Deep *Sph* | 18.34 | 9.92 | 39.08 | 12.63 | 8.16 | 4.77 | 7.11 | 0.0 |
| | | Canadian Char | 17.71 | 6.27 | 23.81 | 9.02 | 17.72 | 8.14 | 17.33 | 7.4 |
| | | Minnesota Char | 23.34 | 10.43 | 25.75 | 10.04 | 14.79 | 4.32 | 11.32 | 2.3 |
| | | Michigan Char | 28.86 | 3.32 | 13.06 | 5.68 | 23.04 | 7.96 | 18.09 | 24.4 |
| | Field Samples | Seney 1 | 41.84 | 4.03 | 18.64 | 4.42 | 13.77 | 3.77 | 13.52 | 13.2 |
| | | Seney 2 | 24.70 | 5.87 | 16.87 | 7.06 | 19.13 | 9.54 | 16.82 | 9.4 |
| | | Seney 3 | 30.88 | 2.24 | 11.92 | 8.68 | 21.24 | 9.11 | 15.93 | 17.4 |
| | | Sleeper Lake 1 | 32.45 | 1.20 | 7.60 | 9.15 | 21.93 | 6.07 | 21.60 | 22.1 |
| | | Sleeper Lake 2 | 36.28 | 4.96 | 11.93 | 1.67 | 18.88 | 6.07 | 20.20 | 17.0 |
| | | Sleeper Lake 3 | 34.49 | 2.65 | 10.64 | 9.10 | 17.35 | 2.20 | 23.56 | 17.0 |
| | | Painesdale 1 | 13.91 | 4.92 | 40.16 | 12.10 | 18.04 | 3.84 | 7.03 | 14.5 |
| | | Painesdale 2 | 16.90 | 5.08 | 38.13 | 14.40 | 14.81 | 3.51 | 7.16 | 9.0 |
| Cross polarisation NMR | Endmembers | Surface *Sph* | 12.67 | 9.06 | 43.51 | 9.52 | 11.21 | 4.65 | 9.38 | 0.0 |
| | | Deep *Sph* | 12.90 | 11.48 | 44.12 | 9.31 | 10.92 | 4.66 | 6.61 | 0.0 |
| | | Canadian Char | 16.53 | 14.39 | 21.00 | 9.38 | 18.74 | 6.52 | 13.44 | 0.0 |
| | | Minnesota Char | 26.16 | 9.36 | 36.49 | 7.67 | 10.53 | 2.97 | 6.82 | 1.3 |
| | | Michigan Char | 37.58 | 6.93 | 13.44 | 3.49 | 19.32 | 8.05 | 11.22 | 16.2 |
| | Field Samples | Seney 1 | 57.31 | 7.03 | 10.59 | 5.42 | 12.43 | 3.63 | 3.59 | 8.4 |
| | | Seney 2 | 25.00 | 14.52 | 23.07 | 6.30 | 16.87 | 6.81 | 7.45 | 0.0 |
| | | Seney 3 | 32.40 | 7.89 | 17.32 | 4.50 | 17.75 | 7.79 | 12.35 | 8.2 |
| | | Sleeper Lake 1 | 27.27 | 11.67 | 23.11 | 7.81 | 16.85 | 4.94 | 8.35 | 3.8 |
| | | Sleeper Lake 2 | 33.37 | 10.97 | 20.81 | 6.53 | 16.73 | 6.19 | 5.40 | 4.7 |
| | | Sleeper Lake 3 | 26.43 | 14.88 | 24.67 | 5.57 | 14.96 | 5.92 | 7.59 | 0.0 |
| | | Painesdale 1 | 28.47 | 12.75 | 21.91 | 6.17 | 19.56 | 6.35 | 4.80 | 5.3 |
| | | Painesdale 2 | 28.94 | 16.36 | 15.89 | 6.34 | 19.91 | 7.76 | 4.80 | 0.0 |

Table A3. Elaboration upon Table A2, providing additional data on direct polarisation NMR chemical shift regions, and on C and N concentrations.

| Samples | C (%) | C (mg g$^{-1}$) | N (%) | N (mg g$^{-1}$) | C (mg) | Relative peak areas for chemical shift regions | | | | | | | | |
|---|---|---|---|---|---|---|---|---|---|---|---|---|---|---|
| | | | | | | Alkyl C 0–45 | O-Alkyl C | | | Aryl C | | Carboxyl C/Amide/Ester | | |
| | | | | | | | Methoxyl /N-alkyl 45–60 | O-Alkyl 60–95 | Di-O-Alkyl 95–110 | Aromatic 110–145 | Phenolic 145–165 | Carboxyl/ Amide 165–185 | Aldehyde/ Ketone 185–220 | 165–220 |
| Surface *Sph* | 44.43 | 444.27 | 0.91 | 9.12 | 0.07 | 16.89 | 8.43 | 34.35 | 12.45 | 12.24 | 6.81 | 7.18 | 1.65 | 8.83 |
| Deep *Sph* | 43.66 | 436.60 | 0.91 | 9.06 | 0.08 | 18.34 | 9.92 | 39.08 | 12.63 | 8.16 | 4.77 | 6.41 | 0.70 | 7.11 |
| Canadian Char | 42.46 | 424.57 | 1.35 | 13.51 | 0.07 | 17.71 | 6.27 | 23.81 | 9.02 | 17.72 | 8.14 | 10.18 | 7.15 | 17.33 |
| Minnesota Char | 45.32 | 453.19 | 1.69 | 16.86 | 0.09 | 23.34 | 10.43 | 25.75 | 10.04 | 14.79 | 4.32 | 9.98 | 1.34 | 11.32 |
| Michigan Char | 48.90 | 489.02 | 3.73 | 37.32 | 0.11 | 28.86 | 3.32 | 13.06 | 5.68 | 23.04 | 7.96 | 9.03 | 9.06 | 18.09 |
| Seney 1 | 53.19 | 531.90 | 1.75 | 17.46 | 0.11 | 41.84 | 4.03 | 18.64 | 4.42 | 13.77 | 3.77 | 9.79 | 3.73 | 13.52 |
| Seney 2 | 53.02 | 530.18 | 1.89 | 18.90 | 0.10 | 24.70 | 5.87 | 16.87 | 7.06 | 19.13 | 9.54 | 11.20 | 5.62 | 16.82 |
| Seney 3 | 53.41 | 534.09 | 1.67 | 16.74 | 0.10 | 30.88 | 2.24 | 11.92 | 8.68 | 21.24 | 9.11 | 12.25 | 3.68 | 15.93 |
| Sleeper Lake 1 | 53.26 | 532.56 | 1.82 | 18.23 | 0.10 | 32.45 | 1.20 | 7.60 | 9.15 | 21.93 | 6.07 | 12.20 | 9.40 | 21.60 |
| Sleeper Lake 2 | 52.37 | 523.69 | 2.02 | 20.15 | 0.09 | 36.28 | 4.96 | 11.93 | 1.67 | 18.88 | 6.07 | 15.05 | 5.15 | 20.20 |
| Sleeper Lake 3 | 50.33 | 503.25 | 2.18 | 21.76 | 0.10 | 34.49 | 2.65 | 10.64 | 9.10 | 17.35 | 2.20 | 11.11 | 12.45 | 23.56 |
| Painesdale 1 | 48.42 | 484.20 | 1.16 | 11.57 | 0.09 | 13.91 | 4.92 | 40.16 | 12.10 | 18.04 | 3.84 | 5.60 | 1.43 | 7.03 |
| Painesdale 2 | 49.56 | 495.64 | 1.32 | 13.17 | 0.09 | 16.90 | 5.08 | 38.13 | 14.40 | 14.81 | 3.51 | 5.69 | 1.47 | 7.16 |

Table A4. Elaboration upon Table A2, providing additional data on cross polarisation NMR chemical shift regions, and on C and N concentrations.

| Source | C (%) | C (mg g⁻¹) | N (%) | N (mg g⁻¹) | C (mg) | Alkyl C 0–45 | Methoxyl/ N-alkyl 45–60 | O-Alkyl 60–95 | Di-O-Alkyl 95–110 | Aromatic 110–145 | Phenolic 145–165 | Carboxyl/ Amide 165–185 | Aldehyde/ Ketone 185–220 | 165–220 |
|---|---|---|---|---|---|---|---|---|---|---|---|---|---|---|
| | | | | | | | **O-Alkyl C** | | | **Aryl C** | | **Carboxyl C/Amide/Ester** | | |
| Surface *Sph* | 44.43 | 444.27 | 0.91 | 9.12 | 0.07 | 12.67 | 9.06 | 43.51 | 9.52 | 11.21 | 4.65 | 5.85 | 3.53 | 9.38 |
| Deep *Sph* | 43.66 | 436.60 | 0.91 | 9.06 | 0.08 | 12.90 | 11.48 | 44.12 | 9.31 | 10.92 | 4.66 | 4.95 | 1.66 | 6.61 |
| Canadian Char | 42.46 | 424.57 | 1.35 | 13.51 | 0.07 | 16.53 | 14.39 | 21.00 | 9.38 | 18.74 | 6.52 | 6.82 | 6.62 | 13.44 |
| Minnesota Char | 45.32 | 453.19 | 1.69 | 16.86 | 0.09 | 26.16 | 9.36 | 36.49 | 7.67 | 10.53 | 2.97 | 5.66 | 1.16 | 6.82 |
| Michigan Char | 48.90 | 489.02 | 3.73 | 37.32 | 0.11 | 37.58 | 6.93 | 13.44 | 3.49 | 19.32 | 8.05 | 8.08 | 3.14 | 11.22 |
| Seney 1 | 53.19 | 531.90 | 1.75 | 17.46 | 0.11 | 57.31 | 7.03 | 10.59 | 5.42 | 12.43 | 3.63 | 3.54 | 0.05 | 3.59 |
| Seney 2 | 53.02 | 530.18 | 1.89 | 18.90 | 0.10 | 25.00 | 14.52 | 23.07 | 6.30 | 16.87 | 6.81 | 5.99 | 1.46 | 7.45 |
| Seney 3 | 53.41 | 534.09 | 1.67 | 16.74 | 0.10 | 32.40 | 7.89 | 17.32 | 4.50 | 17.75 | 7.79 | 8.57 | 3.78 | 12.35 |
| Sleeper Lake 1 | 53.26 | 532.56 | 1.82 | 18.23 | 0.10 | 27.27 | 11.67 | 23.11 | 7.81 | 16.85 | 4.94 | 5.26 | 3.09 | 8.35 |
| Sleeper Lake 2 | 52.37 | 523.69 | 2.02 | 20.15 | 0.09 | 33.37 | 10.97 | 20.81 | 6.53 | 16.73 | 6.19 | 5.27 | 0.13 | 5.40 |
| Sleeper Lake 3 | 50.33 | 503.25 | 2.18 | 21.76 | 0.10 | 26.43 | 14.88 | 24.67 | 5.57 | 14.96 | 5.92 | 6.25 | 1.34 | 7.59 |
| Painesdale 1 | 48.42 | 484.20 | 1.16 | 11.57 | 0.09 | 28.47 | 12.75 | 21.91 | 6.17 | 19.56 | 6.35 | 3.67 | 1.13 | 4.80 |
| Painesdale 2 | 49.56 | 495.64 | 1.32 | 13.17 | 0.09 | 28.94 | 16.36 | 15.89 | 6.34 | 19.91 | 7.76 | 4.44 | 0.36 | 4.80 |

Note: Columns grouped under "Relative peak areas for chemical shift regions".

Table A5. The roster of peaks fitted to each sample spectrum, specified by identifier (Peak), wavenumber (WN), associated moieties and bonds, according to Colthup (1950), Sekiguchi *et al*. (1983), Niemeyer *et al*. (1992), Cocozza *et al*. (2003) and Skoog (2014). Also included is the sign of the relationship, positive (+) or negative (-), to pyrogenic carbon in models fitted for both direct polarisation (DP) and cross polarisation (CP) estimations. Superscripts indicate bonds and moieties supported by ([1]) Niemeyer *et al*. 1992 and ([2]) Cocozza *et al*. (2003), who concern themselves specifically with peat samples. Cells shaded grey indicate when a peak was used as a parameter in an overall model. P values and LogWorths are indicated in the context of the overall models.

| Peak | Peak WN $(cm^{-1})$ | Relation w/PyC (DP) | Relation w/PyC (CP) | P value (LogWorth) (DP) | P value (LogWorth) (CP) | Associated moieties | Associated bonds |
|---|---|---|---|---|---|---|---|
| 1 | $1054 \pm 1.84$ | 0 | 0 | | | Aromatics, Ethyl & propyl alkanes, Primary alcohols, Aliphatic aldehydes, Polysaccharides[2] | C-C, C-O[2], C-N |
| 2 | $1116 \pm 1.29$ | 0 | 0 | | | Aromatics, Anhydrides, Isopropyl alkanes, Aliphatic ethers, Secondary alcohols, Amides, Amines, Benzoate / phyhalate esters | C-C, C-O, C-N |
| 3 | $1160 \pm 0.94$ | + | + | 0.0003 (3.471) | < 0.0001 (4.708) | Aromatics, Aliphatics[1], Amides, Amines, Esters, Ketones, Iso-propyl and Tertiary butyl alkanes | C-C, C-O, C-N, -C-OH[1] |
| 4 | $1229 \pm 2.77$ | 0 | - | | 0.0173 (1.763) | Acetate, Cyclic anhydrides, Aromatic alcohols, Aromatic ketones, ethers[2], carboxyls[1,2] | C-O[1,2], C-N, O-H, -CH[1] |
| 5 | $1267 \pm 1.45$ | 0 | 0 | | | Cyclic anhydrides, Aromatic ethers, Aromatic alcohols, Aromatic ketones, Esters, Tertiary butyl alkanes, Phenolic OH[1], ethers[2], carboxyls[2] | C-O[2], C-N, O-H,-C-OH[1] |
| 6 | $1326 \pm 0.77$ | 0 | 0 | | | Alkanes, Alkenes, Alcohols, Amines | C-H, O-H |
| 7 | $1381 \pm 0.02$ | - | - | < 0.0001 (4.415) | 0.0001 (3.931) | Alkanes, Tertiary alcohols, Aromatic alcohols, Aldehydes, Phenolic OH[2], Aliphatic OH[2] | C=S, C-H, O-H[2] |
| 8 | $1431 \pm 0.76$ | 0 | 0 | | | Alkanes, Alkenes, Carboxylic acids, Alcohols, Phenolic OH[2], Aliphatic OH[2] | C-H, O-H[2] |
| 9 | $1460 \pm 0.68$ | 0 | 0 | | | Alkanes, Primary Alcohols, Vicinal trisubstituted aromatics, Methyl[1], Methylene[1] | C-H[1] |
| 10 | $1512 \pm 3.30$ | 0 | 0 | | | Aromatics[2], Amides[2], Amines[2], Imines[2] | N-H, C=C[1,2], C=N[2] |
| 11 | $1615 \pm 1.19$ | 0 | 0 | | | Alkenes, Aromatics[2], Ionised carboxyl[2], Amides, Amines, HCl, Covalent nitrate, Covalent nitrite | C=N, C=C[2], N-H, -COO[-1,2] |
| 12 | $1720 \pm <0.01$ | + | + | < 0.0001 (13.564) | < 0.0001 (7.021) | Anhydrides, Esters, Aldehydes[2], Ketones[2], Covalent carbonates, Carboxyl[2], Carbonyl[2] | C=O[1,2] |
| 13 | $2852 \pm 1.78$ | 0 | 0 | | | Alkanes, Aldehydes, Aliphatic CH[2] | C-H[1,2] |
| 14 | $2921 \pm 1.65$ | - | 0 | < 0.0001 (4.489) | | Alkanes, Alkenes, Carboxylic acids, Aliphatic CH[2] | C-H[2] |
| 15 | $3425 \pm <0.01$ | 0 | 0 | | | Alcohols, Amines, Amides | O-H[2], N-H |
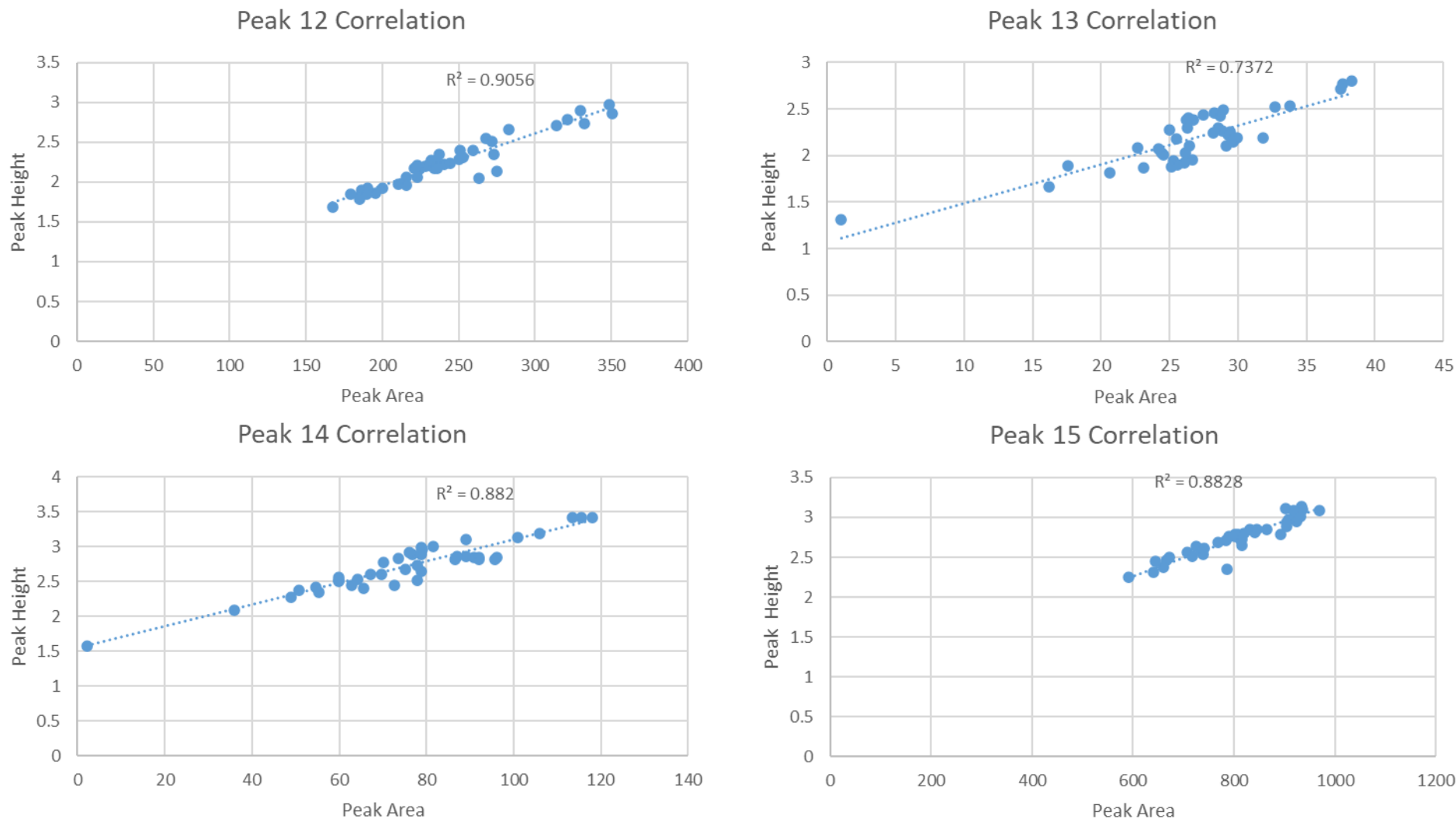
Figure A1. Correlations between the peak areas fit in OriginPro 2019b and the peak heights found in the corresponding FTIR spectra in the region between 4000 and 2000 cm⁻¹ of the spectra shown in Figure 2. Despite the appearance of lack of fit in Figure 2, there are strong correlations. Both axes are unitless because all spectra were standardised for analysis.